Brief Report

DOI: 10.5582/irdr.2024.01029

Genetic analysis of a novel *FBN1* mutation in a pediatric Marfan syndrome patient

Xiangdong Zhang[1,§], Lixing Zhou[2,§], Jiao Liu[1], Qunda Shan[1], Zhaoxia Song[1], Fang Zhou[1], Lifang Liu[1], Xia Luo[1,*]

[1] Lishui Maternal and Child Health Care Hospital, Lishui, Zhejiang, China;
[2] Department of Optometry and Ophthalmology College, Wenzhou Medical University, Wenzhou, Zhejiang, China.

SUMMARY The aim of this study was to investigate a novel *FBN1* gene mutation in a pediatric patient with Marfan syndrome (MFS) to provide a theoretical basis for genetic counseling. The subject was a 5-month-old male infant. With informed consent from the proband and his family, 2 mL of peripheral venous blood was collected from the patient, his father, mother, and sister. DNA was extracted using a DNA extraction kit with EDTA-K as an anticoagulant. The extracted DNA was subjected to minigene transcription and bioinformatics analysis. For minigene construction, wild-type and mutant minigenes were inserted into pcMINI and pcMINI-C vectors, respectively. Four recombinant vectors were transfected into the HeLa and 293T cell lines. After transfection for 48 hours, RNA was extracted from eight samples. DNA was also extracted from the family members' samples to construct a library. Target regions were captured using the SureSelect Human All Exon V6 (Agilent) kit and were sequenced with Illumina NovaSeq (sequencing read length 2×150 bp). Bioinformatic analysis identified the c.8226+5del mutation as a variant of uncertain clinical significance (VOUS). Literature and database reviews confirmed that this mutation had not been previously reported, identifying it as a novel mutation. The study identified a novel *FBN1* mutation, c.8226+5del, that may be associated with clinical features such as low-set ears and distinctive facial characteristics in the proband. This mutation likely affects normal mRNA splicing, altering the structure and function of Exon 64 and potentially contributing to the development of autosomal dominant MFS.

Keywords Marfan syndrome (MFS), *FBN1*, mutation, novel, gene mutation

1. Introduction

Marfan syndrome (MFS) is a hereditary connective tissue disorder that is inherited in an autosomal dominant manner. The overall incidence of this disease is relatively low, approximately 0.01% to 0.02%, with 20% to 30% of cases arising from de novo mutations. Incidence among live-born infants is about 0.01% (*1,2*). Although the incidence in live-born infants is low, the clinical symptoms are often severe, leading to a poor prognosis, and most affected children do not survive beyond 17 months. The primary characteristics of MFS include skeletal, ocular, and cardiovascular abnormalities. This disease is closely associated with age, and patients typically exhibit features such as a tall and slender stature, elongated limbs, angina, arachnodactyly, arrhythmias, spinal abnormalities, and retinal detachment (*3*). If not promptly managed, the disease can also affect the skin, lungs, and central nervous system (*4*). Currently, the Ghent criteria are the gold standard for the diagnosis and treatment of MFS. However, the genetic, environmental, and physical characteristics of patients can vary significantly, resulting in diverse clinical presentations and diagnostic challenges (*5*).

In the 1990s, Dietz and colleagues proposed that mutations in the fibrillin-1 (*FBN1*) are a significant factor in the development of MFS (*6*). More recent research has confirmed that *FBN1* is the causative gene for MFS (*7*). The current study analyzed the *FBN1* gene in a pediatric MFS patient using high-throughput sequencing. Results revealed a novel mutation site, further expanding the genetic data associated with this disease.

2. Materials and Methods

2.1. Materials

The subject was a 5-month-old male infant who was delivered *via* cesarean section at 35 weeks and 4 days of gestation due to oligohydramnios. This study adhered to the principles of the Helsinki Declaration and was approved by the Ethics Committee of the Medical School (NO. 2020034). Informed consent was obtained from all participants, with consent for those under 18 years of age being provided by their guardians.

2.2 Methods

2.2.1. Specimen collection

After obtaining informed consent from the proband's family, 2 mL of peripheral venous blood was collected from the patient, his father, mother, and sister. The blood samples were collected in EDTA-K tubes to prevent coagulation. DNA was extracted from the samples using a DNA extraction kit (QIAGEN, Germany) following standard procedures.

2.2.2. Methods of detection

2.2.2.1. Introduction of restriction sites into minigenes

Leukocyte gDNA was extracted using a DNA extraction kit, and DNA was amplified using a PCR machine. The primers used for the reaction are listed in Table 1. Each PCR tube contained 22 μL of 1.1× Mix, 1 μL of upstream primer (Primer-F), 1 μL of downstream primer (Primer-R), and 1 μL (0.5 μg) of gDNA, with RNase-free water added to reach a final volume of 30 μL. PCR amplification was performed with an annealing temperature of 57℃ for 30 cycles. The PCR products were then separated by gel electrophoresis, and the desired bands were excised and purified.

2.2.2.2. Construction of recombinant vectors

The construction of recombinant vectors involved restriction digestion, ligation, transformation, and verification of recombinant clones.

Restriction digestion of recombinant vectors: To the DNA fragment (25 μL, 500 ng), 3 μL of 10× NEB buffer, 0.6 μL each of Enzyme 1 and Enzyme 2, and ddH_2O were added to reach a final volume of 30 μL. The mixture was incubated at 37℃ for 2 hours. After digestion, the recombinant vector was verified with gel electrophoresis and the desired bands were excised for purification.

Construction of recombinant vectors: Seven μL of the digested DNA fragment (wild-type/mutant), 1 μL of 10× ligase buffer, 1 μL of digested vector, and 1 μL of ligase were combined. The mixture was incubated at 4℃ overnight for ligation. The ligated product was transformed into E. coli DH5α competent cells and incubated at 37℃ overnight. Several single colonies were randomly selected for identification. Verification methods included colony/liquid PCR and Sanger sequencing.

2.2.2.3. Cell transfection

The recombinant vectors were transiently transfected into the HeLa and 293T cell lines following the instructions provided by the lipofection reagent manufacturer. Samples were collected 48 hours post-transfection.

2.2.2.4. Minigene transcription analysis

Total RNA was extracted from the transfected cell samples according to the kit instructions. After determining the RNA concentration, equal amounts of RNA were reverse transcribed into cDNA. PCR amplification was performed using flanking primers specific to the minigene vector. The resulting gene transcription bands were detected with agarose gel electrophoresis. Each band was then excised and subjected to Sanger sequencing for further analysis.

2.2.3. Bioinformatic analysis

Quality control of the raw data was performed using the software FastQC. The filtered sequencing reads were

Table 1. Experimental primers

Primer name	Primer sequence (5′-3′)
231081-*FBN1*-F	TGGCCTCTCCGAATCACTAG
231361-*FBN1*-F	GGCCCTAGTGGTTTTGAATG
234049-*FBN1*-R	CCAATGGAAATACACGTCCC
234456-*FBN1*-R	GCACCATTACAAACCCTCAC
pcMINI-*FBN1*-KpnI-F	GGTAGGTACCTACATGGCCTCCCTCATCTA
pcMINI-*FBN1*-EcoRI-R	TGCAGAATTCCTCCACGTTATTTTTGTCTA
FBN1-mut-R	GAAACTAACTTCTGACCACCTCGATATTGG
FBN1-mut-F	CCAATATCGAGGTGGTCAGAAGTTAGTTTC
pcMINI-C-*FBN1*-KpnI-F	GGTAGGTACCAGGGAACTGGGAATTAGAGG
pcMINI-C-*FBN1*-EcoRI-R	TGCAGAATTCTTAATGAAGCAAAACCTGGA

aligned to the GRCh37/hg19 reference genome using the software BWA (version 0.7.15-hg19). Duplicate sequences were removed with the software Picard. Single nucleotide variants (SNVs) and insertion-deletion variants (Indels) were detected using the GATK toolkit (version 3.7-0). Copy number variations (CNVs) were identified using XHMM (version 1.0) and CNVkit (version 0.8.4). Annotation of the variants was carried out using the software Annovar and VEP.

2.2.4. Quality control analysis

2.2.4.1. Data quality control

Throughout the detection and analysis process, quality control analysis of the samples was performed. Unqualified samples were excluded. Key metrics recorded included Q20, Q30, GC content, average sequencing depth, and coverage of the targeted regions.

2.2.4.2. Sample identification

In this study, high-frequency SNP loci (8–10) were used as sample identification markers to prevent sample damage and cross-contamination during testing. NGS experiments were conducted and SNP locus analysis was performed simultaneously to ensure that the test samples were free from cross-contamination.

2.2.5. Pathogenic variant filtering and selection

2.2.5.1. Filtering of high-frequency SNVs/Indels

High-frequency mutations (MAF > 0.01, MAF > 0.05) were filtered out using population genetic variant databases such as dbSNP, 1000 Genomes, ExAC, and gnomAD, along with a local database. For unique cases, personalized threshold screening was used.

2.2.5.2. Classification of SNVs/Indels and selection of candidate gene variants

According to ACMG standards, variants are classified into five categories: pathogenic (P), likely pathogenic (LP), variants of uncertain significance (VOUS), likely benign (LB), and benign (B). Using these guidelines, in-depth studies of suspected pathogenic mutations that matched the expression profile of the proband we conducted using Sanger sequencing. However, three types of SNVs/Indels were excluded from the final report:

(1) Mutations likely to be benign (as per ACMG guidelines).

(2) VOUS gene mutations inherited in a dominant manner from asymptomatic parents.

(3) Potentially pathogenic mutations that did not meet the patient's clinical criteria (as per ACMG guidelines).

2.2.6. Filtering and interpretation of known or potentially clinically significant CNVs

CNVs were interpreted according to ACMG guidelines. CNVs classified as benign or likely benign were not included in the report. With the assent of the testing laboratory, submitting personnel can retrieve information on the CNVs from the list of excluded variants.

3. Results and Discussion

3.1. Physical examination results

The patient was a 5-month-old male, delivered *via* cesarean section at 35 weeks and 4 days of gestation due to oligohydramnios. Physical examination findings included: distinct facial features, prominent eyes, downward slanting palpebral fissures, a broad forehead, low-set ears, visible veins on the skin, and a normal height. A fundus examination revealed retinal white spots and pigment deposition in the left lens.

The patient's mother has had a visual acuity of 0.2–0.4 since childhood without correction, a broad forehead, prominent eyes, low-set ears, abnormally shaped auricles, pectus carinatum, pelvic abnormalities, long fingers with visible surface veins, and irregular teeth alignment. A fundus examination revealed partial lens dislocation and surface pigment deposition.

The patient's sister, born to the same parents, has amblyopia in one eye but otherwise normal facial features.

3.2. Analysis of transcription results

The minigenes, both wild-type and mutant, were inserted into the pcMINI and pcMINI-C vectors. These four recombinant vectors were then transfected into the HeLa and 293T cell lines. After transfection for 48 hours, RNA was extracted from a total of eight samples.

3.2.1. Analysis of pcMINI series results

The minigene construction strategy for pcMINI-*FBN1*-wt/mut involved inserting part of Intron 63 (346 bp), Exon 64 (175 bp), and part of Intron 64 (439 bp) into the pcMINI vector. This vector contains the universal ExonA-intronA-MCS-intronB-ExonB sequence. After transfecting the cells, the splicing of ExonA-Exon64-ExonB was observed for abnormalities. The results are shown in Figure 1.

RT-PCR results indicated that in both HeLa and 293T cells, the wild-type minigene produced a single band of the expected length, 564 bp, named band a. The mutant minigene produced two smaller bands than the wild-type, named band b and band c. Sanger sequencing was

performed on band a from the wild-type and bands b and c from the mutant minigenes in both cell lines.

Sequencing results revealed that wild-type band a represented normal splicing, with the structure ExonA (192 bp) - Exon64 (175 bp) - ExonB (57 bp). Mutant band b exhibited abnormal splicing, with the structure ExonA (192 bp) - ΔExon64 (101 bp) - ExonB (57 bp). Mutant band c also exhibited abnormal splicing, with Exon64 skipped, resulting in the structure ExonA (192 bp) - ExonB (57 bp).

3.2.2. Analysis of pcMINI-C series results

The minigene construction strategy for pcMINI-C-*FBN1*-wt/mut involved inserting part of Intron 63 (186 bp), Exon 64 (175 bp), Intron 64 (1,189 bp), and Exon 65 (390 bp) into the pcMINI-C vector, which contains the universal ExonA-IntronA-MCS sequence. After transfecting the cells, the splicing of ExonA-Exon64-Exon65 was observed for abnormalities. The results are shown in Figure 2.

RT-PCR results indicated that in both HeLa and 293T cells, the wild-type minigene produced a single band of the expected length, 936 bp, named band a. The mutant minigene produced two smaller bands than the wild-

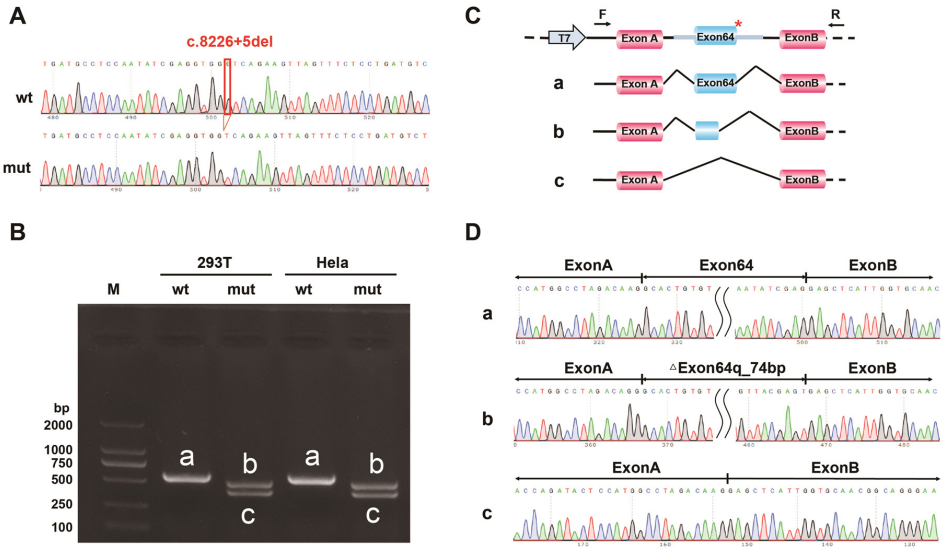

Figure 1. Detection of the pcMINI vector. (A) Sequencing diagram of minigene construction, with wt (wild type) shown on top and mut (mutation) shown below; **(B)** Gel electrophoresis of the results of RT-PCR transcription analysis, with bands labeled as a, b, c in HeLa and 293T cells; **(C)** Schematic diagram illustrating the minigene construction strategy and splicing pattern; **(D)** Sequencing results corresponding to splicing bands. The red asterisk (*) indicates the mutation site.

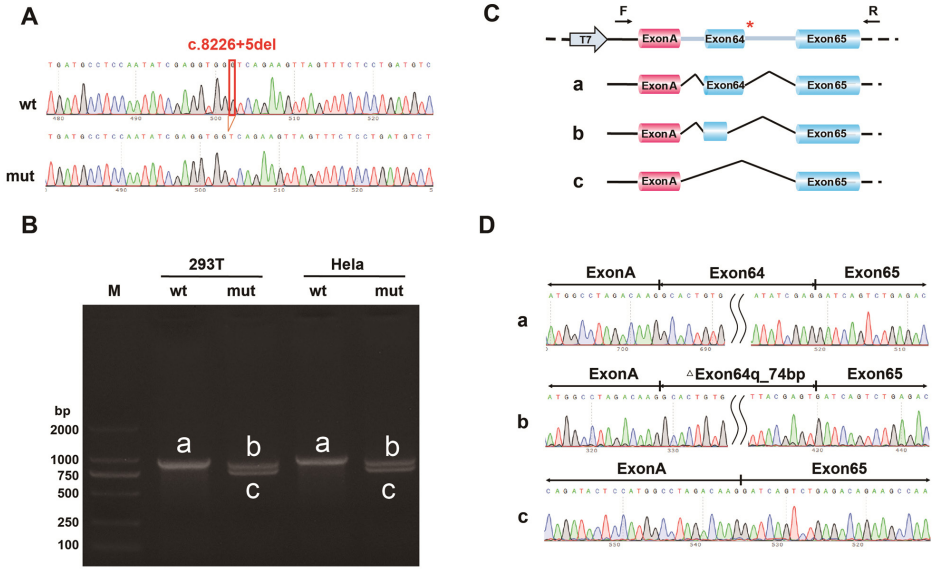

Figure 2. Detection of the pcMINI-C vector. (A) Sequencing diagram of minigene construction, with wt (wild type) shown on top and mut (mutation) shown below; **(B)** Gel electrophoresis of the results of RT-PCR transcription analysis, with bands labeled as a, b, c in HeLa and 293T cells; **(C)** Schematic diagram illustrating the minigene construction strategy and splicing pattern; **(D)** Sequencing results corresponding to splicing bands. The red asterisk (*) indicates the mutation site.

type, named band b and band c. Sanger sequencing was performed on wild-type band a and mutant bands b and c.

Sequencing results revealed that wild-type band a represented normal splicing, with the structure ExonA (192 bp) - Exon64 (175 bp) - Exon65 (390 bp). Mutant band b exhibited abnormal splicing, with the structure ExonA (192 bp) - ΔExon64 (101 bp) - Exon65 (390 bp). Mutant band c also exhibited abnormal splicing, with Exon64 skipped, resulting in the structure ExonA (192 bp) - Exon65 (390 bp).

The *in vitro* minigene assay results indicated that the c.8226+5del mutation affects normal mRNA splicing. Both pcMINI and pcMINI-C vector assays yielded consistent results. The c.8226+5del mutation led to the deletion of 74 bp on the right side of Exon64, resulting in the cDNA and protein sequence c.8153_8226del p.Cys2718*, where a premature termination codon (PTC) was introduced in Exon64 and a truncated protein of 2,717 aa was produced. In addition, the c.8226+5del mutation caused the skipping of Exon64, resulting in the cDNA and protein sequence c.8052_8226del p.His2685Ile fs*9, where a PTC was introduced in Exon65 and a truncated protein of 2,692 aa was produced.

3.3. Sequencing results of *FBN1* gene variant c.8226+5del

DNA was extracted from samples of the tested family, and a library was constructed. Target regions were captured using the SureSelect Human All Exon V6 (Agilent) hybridization capture kit, followed by high-throughput sequencing using Illumina NovaSeq (sequencing read length: 2×150 bp). Through bioinformatic analysis, the variant c.8226+5del that was detected in genetic testing was classified as a VOUS (as shown in Table 2, Figures 3 and 4).

A significant characteristic of MFS is multiple systemic developmental mutations in the human body. Approximately 80% of patients clinically manifest with lens dislocation or subluxation, and in severe cases, they may also develop complications such as aortic aneurysm, contributing to a high mortality rate among patients. *FBN1* is located on 15q21.1, spans 235 kb, and encodes fibrillin-1, consisting of 65 exons. Fibrillin-1, a glycoprotein with a molecular weight of 350,000 that consists of 2871 aa, forms the extracellular matrix primarily in elastic or inelastic tissues (*8, 9*). The protein is predominantly distributed in systemic elastic tissues, including the skin, tendons, lungs, cardiovascular system, and the suspensory ligament of the lens. According to the HGMD database, there were approximately 2,000 confirmed *FBN1* gene mutation sites prior to 2018, with 67% being missense mutations (*10*). Clinical manifestations of MFS are influenced by the location and type of *FBN1* gene mutations (*11*).

MFS exhibits significant clinical heterogeneity, primarily affecting the skeletal, ocular, and

Table 2. Sequencing results for *FBN1* gene variant c.8226+5del

Sequencer	Volume of sequencing data	Average depth of target region	20× coverage (%)	Q30(%)	Sequencing platform
Patient	15.51G	159.7X	96.91	92.43	Illumina NovaSeq (2×150bp)
Mother of the patient	16.33G	175.13X	97.22	94.45	
Father of the patient	18.37G	205.54X	97.90	94.46	

Figure 3. IGV schematic diagram of sequencing results for *FBN1* gene variant c.8226+5del. (A), Patient; **(B),** Mother of the patient; **(C),** Father of the patient.

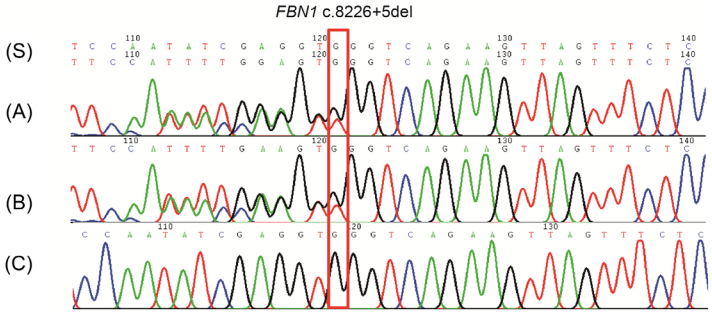

Figure 4. Schematic representation of Sanger sequencing validation results for *FBN1* gene variant c.8226+5del in the patient and parents. (S), Sequencer; **(A),** Patient; **(B),** Mother of the patient; **(C),** Father of the patient.

cardiovascular systems. Major clinical manifestations include dolichocephaly, underdeveloped cheekbones, micrognathia, distinctive facial features, aortic aneurysm-like dilation, aortic valve regurgitation, aortic dissection, mitral valve prolapse, arachnodactyly, spider-like fingers and toes, chest deformities, pes planus, ectopia lentis, myopia, and retinal detachment (*12*). In addition, patients may also present with abnormalities in the lungs, skin, and central nervous system. Due to the lack of uniform clinical features of MFS, there is currently limited in-depth research on expression of the disease genotype (*13*). However, studies have confirmed that the pathogenesis of MFS is associated with *FBN1* mutations, leading to systemic connective tissue diseases that significantly impact the quality of life and daily activities of patients. Moreover, the disease is hereditary, and some patients may experience respiratory or circulatory failure crises or even death, causing serious physical and psychological harm to the affected children and their families (*14*). Therefore, genetic screening for patients (those with hereditary MFS, carriers, and infants with cardiovascular malformations) is of great significance. A positive screening result requires special attention, timely notification of the patient and their family, explanation of disease development and prognosis, enhanced cooperation between patients and healthcare providers, and prevention of the further progression of the disease and complications. There may be two causes of *FBN1* gene mutations: mutations occurring during embryonic development and parental germline mosaicism (*15*). Germline mosaicism refers to mutations occurring only during early embryonic germ cell growth. This cell lineage accounts for a small proportion of the peripheral blood genome, and most of the other body cells, except for a small part of the germ cells, do not carry mutations, resulting in a low detection efficiency. Therefore, families of patients with this feature require prenatal genetic diagnosis (*16, 17*). The *FBN1* gene mutation c.8226+5del that was detected in this study has not been reported in the literature and is classified as a VOUS. MFS caused by this gene is often inherited in an autosomal dominant manner. Family testing results confirmed that the mother of the patient also carried this mutation, and the clinical phenotype of the mother was similar to that of the patient. However, whether c.8226+5del is the key gene for the onset of MFS, and the changes in Exon64 caused by this gene mutation and the resulting alterations in protein function, is currently unknown and needs to be studied further for confirmation.

In summary, this study identified a novel variant site, c.8226+5del, in the *FBN1* gene that may be associated with clinical features such as "low-set ears" and a "distinctive facial appearance" in MFS patients. This mutation may affect the normal splicing of gene mRNA, leading to changes in the structure and function of Exon64, thereby causing autosomal dominant inherited MFS. These findings could provide insights for subsequent clinical research and genetic testing.

Funding: This work was a Self-funded Project for Applied Research on Public Welfare Technology of the City of Lishui (2021SJZC053).

Conflict of Interest: The authors have no conflicts of interest to disclose.

References

1. Kang XC, Xu Y, Lin AQ, Feng XC, Han X. Research progress on the relationship between *FBN1* gene and Marfan syndrome and its related phenotypes. J Clin Internal Med. 2021; 38:724-727. (in Chinese)
2. Xu S, Li L, Fu Y, Wang X, Sun H, Wang J, Han L, Wu Z, Liu Y, Zhu J, Sun L, Lan F, He Y, Zhang H. Increased frequency of *FBN1* frameshift and nonsense mutations in Marfan syndrome patients with aortic dissection. Mol Genet Genomic Med. 2020; 8:e1041.
3. Iskandar Z, Dodd M, Stuart G, Caputo M, Clayton T, Chin C, Gibb J, Child A, Aragon-Martin JA, Jin XY, Flather M, Huang JTJ, Choy AM. 5 Exaggerated elastin turnover in childhood and adolescence in Marfan syndrome-Correlation with age-New insights from the AIMS trial. Eur Heart J. 2021; 26:A4-A5.
4. Rudagi BM, Rishabh J, Arif M, Namrata C, Shahbaaz N, Gaurav B. Management of unilateral temporomandibular joint ankylosis & orthomorphic correction in a patient with Marfan syndrome: A rare case report. Int J Surg Case Rep. 2020; 75:157-161.

5. Grange T, Aubart M, Langeois M, Benarroch L, Arnaud P, Milleron O, Eliahou L, Gross MS, Hanna N, Boileau C, Gouya L, Jondeau G. Quantifying the genetic basis of Marfan syndrome clinical variability. Genes (Basel). 2020; 11:574.
6. Willis BR, Lee M, Rethanavelu K, Fung JLF, Wong RMS, Hui P, Yeung KS, Lo IFM, Chung BHY. A case of G1013R *FBN1* mutation: A potential genotype-phenotype correlation in severe Marfan syndrome. Am J Med Genet A. 2020; 182:1329-1335.
7. Borsoi J, Farinha-Arcieri LE, Morato-Marques M, Delgado Sarafian R, Pinheiro M, Veiga Pereira L. Generation of genetically modified human induced pluripotent stem cell lines harboring haploin sufficient or dominant negative variants in the *FBN1* gene. Stem Cell Res. 2021; 54:102434.
8. Jensen SA, Atwa O, Handford PA. Assembly assay identifies a critical region of human fibrillin-1 required for 10-12 nm diameter microfibril biogenesis. PLoS One. 2021; 16:e0248532.
9. Tian Y, Hou C, Wang XY, Zhu HX, Cao BB, Li XJ, Chen WX, Liang HC. Report of a case of West syndrome in a Marfan syndrome family with *SLC35A2* gene mutation and literature review. J Clin Ped. 2020; 38:302-305. (in Chinese)
10. Iosef C, Pedroza AJ, Cui JZ, Dalal AR, Arakawa M, Tashima Y, Koyano TK, Burdon G, Churovich SMP, Orrick JO, Pariani M, Fischbein MP. Quantitative proteomics reveal lineage-specific protein profiles in iPSC-derived Marfan syndrome smooth muscle cells. Sci Rep. 2020; 10:20392.
11. Schnause AC, Komlosi K, Herr B, Neesen J, Dremsek P, Schwarz T, Tzschach A, Jägle S, Lausch E, Fischer J, Gläser B. Marfan syndrome caused by disruption of the *FBN1* gene due to a reciprocal chromosome translocation. Genes (Basel). 2021; 12:1836.
12. Stengl R, Bors A, Ágg B, Pólos M, Matyas G, Molnár MJ, Fekete B, Csabán D, Andrikovics H, Merkely B, Radovits T, Szabolcs Z, Benke K. Optimising the mutation screening strategy in Marfan syndrome and identifying genotypes with more severe aortic involvement. Orphanet J Rare Dis. 2020; 15:290.
13. Kakroo S A. Marfan syndrome with CRHD. Indian J Cardiovasc Disease in Women-WINCARS. 2020; 5:322-326.
14. Mendenhall L, Shaver K G, Goebel L J. Bilateral extracranial carotid artery aneurysms: A rare complication of Marfan syndrome. Marshall J Med. 2020; 6:5.
15. Trifirò G, Mora S, Marelli S, Luzi L, Pini A. Increased fracture rate in children and adolescents with Marfan syndrome. Bone. 2020; 135:115333.
16. Bitarafan F, Razmara E, Khodaeian M, Keramatipour M, Kalhor A, Jafarinia E, Garshasbi M. Three novel variants identified in *FBN1* and TGFBR2 in seven Iranian families with suspected Marfan syndrome. Mol Genet Genomic Med. 2020; 8:e1274.
17. Mannucci L, Luciano S, Salehi LB, Gigante L, Conte C, Longo G, Ferradini V, Piumelli N, Brancati F, Ruvolo G, Novelli G, Sangiuolo F. Mutation analysis of the *FBN1* gene in a cohort of patients with Marfan Syndrome: A 10-year single center experience. Clin Chim Acta. 2020; 501:154-164.

Received May 14, 2024; Revised June 26, 2024; Accepted July 5, 2024.

[§]These authors contributed equally to this work.
**Address correspondence to:*
Xia Luo, Department of Health Care, Lishui Maternal and Child Health Care Hospital, Lishui, Zhejiang 323000, China.
E-mail: lssqfm@126.com

Released online in J-STAGE as advance publication July 14, 2024.